Materials Science & Engineering A 957 (2026) 149955

Contents lists available at ScienceDirect

Materials Science & Engineering A

journal homepage: www.elsevier.com/locate/msea

Improving the ductility of 2.6-GPa high-carbon martensitic steel by prior bainitic transformation

Sien Liu [a,*], Koyo Shimizu [a], Jiaqiang Dang [a], Karel Blanken [a], Fabien Briffod [b], Shoichi Nambu [a,**]

[a] Department of Materials Engineering, Graduate School of Engineering, The University of Tokyo, 7-3-1, Hongo, Bunkyo-ku, Tokyo, 113-8656, Japan
[b] Research Center for Structural Materials, National Institute for Materials Science, 1-2-1 Sengen, Tsukuba, 305-0047, Ibaraki, Japan

ARTICLE INFO

Keywords:
Bainite
Prior austenite grain boundary
Ultrahigh strength
High-carbon steel

ABSTRACT

In this study, we designed a lean and time-efficient high-carbon bainite/martensite (B/M) steel with 2.64 GPa ultimate tensile strength and 9% uniform elongation. Prior lower bainite nucleated along prior austenite grain boundaries (PAGBs) suppressed premature intergranular fracture in martensitic constituent. Blocky retained austenite (RA) was observed adjacent to the bainite sheaves along PAGBs. During tensile deformation, significant work hardening behaviour was observed, primarily due to the transformation-induced-plasticity (TRIP) effect of blocky RA. A brittle-to-ductile transition was observed with increasing bainitic transformation time at the early stage. Overall, a low fraction of prior lower bainite can effectively enhance the ductility of the high-carbon martensite without sacrificing its ultrahigh strength.

1. Introduction

Since the increasing demand for developing novel steels with much higher strength and good ductility, several ultrahigh-strength steels have been developed, primarily through applying sever plastic deformation and complex processes [1–4]. However, such complex processes are impractical for industrial applications, emphasizing the desire for simpler approaches, such as heat treatment alone. Increasing carbon content is the most effective strategy for strengthening martensite [5,6]. Nevertheless, high-carbon martensitic steels often exhibit unpredicted brittle fracture, primarily attributed to prior austenite grain boundaries (PAGBs) [7,8]. Moreover, fracture along high-misorientation PAGBs is preferentially facilitated in high-carbon martensite, which is due to their lower grain boundary (GB) adhesion and poor crack resistance [9,10].

As a solution, bainite transformation along PAGBs potentially enhances the local deformability. When lower bainite nucleate from fully austenitized microstructure, bainite sheaves preferentially nucleate along PAGBs with high grain boundary (GB) energy [11]. This provides a strategy for designing bainite/martensite (B/M) steels with superior strength-ductility combinations [12,13]. So far, various routes have been proposed to strengthen B/M steels. For instance, reducing prior austenite grain (PAG) size and lowering bainitic transformation temperature facilitate the formation of finer bainitic laths [14,15], which in turn leads to slower transformation kinetic [16]. As a solution, primary martensite [17,18] and alloying elements design [19] can accelerate bainitic transformation kinetics. Moreover, the presence of prior martensite alters the bainitic nucleation sites from PAGBs [11,20] to martensite boundaries [18,21], which diminishes the enhancement effect on PAGBs. Additionally, Samanta et al. [22] reported that isothermal bainitic transformation can occur below the martensite-start-temperature (Ms). Despite these achievements, an optimized heat treatment strategy to fabricate ultrahigh-strength B/M steels remains challenging.

In B/M steels, premature crack initiation is the primary cause of the reduced toughness [17,23]. Potential crack initiation sites include PAGBs [24], precipitation interfaces [25–27] and phase or substructural boundaries [21,28,29]. Here, the bainite nucleation site plays a critical role in suppressing local premature crack initiation. In addition, the complex B/M substructure within PAGs introduces diverse deformation mechanisms [30]. Therefore, the present study aimed to achieve superior ultrahigh-strength and ductility combination by only heat treatment processes. The deformation behaviour and fracture mechanisms of the high-carbon B/M steels were also investigated.

* Corresponding author. 7-3-1 Hongo, Bunkyo-ku, Tokyo, 113-8656, Japan.
** Corresponding author. 7-3-1 Hongo, Bunkyo-ku, Tokyo, 113-8656, Japan.
E-mail addresses: sien_liu@metall.t.u-tokyo.ac.jp (S. Liu), nambu@metall.t.u-tokyo.ac.jp (S. Nambu).

https://doi.org/10.1016/j.msea.2026.149955
Received 5 June 2025; Received in revised form 12 January 2026; Accepted 19 February 2026
Available online 20 February 2026

2. Materials and methods

In this study, we designed a novel high-carbon steel with the chemical composition listed in Table 1. A carbon content of 0.834 wt% was employed to improve the overall strength. 1.78 wt% of Si was added to suppress the formation of cementite during bainitic transformation [31]. The resulting carbide-free bainite further contributes to strength enhancement due to its high dislocation density and finer microstructure [32]. Mo was employed to enhance GB cohesion for preventing intergranular brittleness. Only low fraction of Mn was employed to decrease the incubation time of bainitic transformation [33].

Fig. 1(a) shows the heat treatment routes. Following soft annealing at 680 ° C for 1 h of hot rolled plate, cold rolling was conducted at room temperature (RT) with a thickness reduction from 12 mm to 1 mm. The steel sheet was subsequently machined into tensile test specimens oriented along the rolling direction (RD), as shown in Fig. 1(b). Then two distinct heat treatment routes were designed for achieving either homogeneous martensite (full M) or bainite/martensite (B/M) microstructure. After austenitizing at 900 ° C for 2 min, the full M specimens were oil quenched to RT, and the B/M specimens were isothermally held at 280° C or 300° C, and then oil quenched. Finally, all specimens were tempered at 200° C for 3 h, followed by air cooling. All heat treatments were performed in Ar atmosphere.

Fig. 1(c) depicts the microstructure evolution of the B/M specimens in various stages. After austenitization (c1), bainitic transformation initiated during the isothermal holding from PAGBs (c2). Subsequent oil quenching resulted in martensitic transformation in the untransformed γ-phase region (c3). The final tempering treatment process relieved the residual stress.

Fig. 1(d) shows the dilatation investigation of an 8 mm-diameter cylindrical specimen under a heating-cooling process. The specimen was heated up at 30 ° C/s, held at 1000° C for 300 s, and finally nitrogen-gas quenched at 20° C/s to room temperature. The austenite transformation temperature is 834° C and the Ms is 125° C. Fig. 1(e) shows the dilatation under isothermal holding at 280 ° C. A rapid expansion period was observed between holding time of 2-4 ks, whereas an initial dilatation from the early stage.

The microstructure was observed using a light optical microscope, field-emission scanning electron microscope (FE-SEM, JOEL JSM-7001F, accelerating voltage of 15 kV) and electron backscattered diffraction (EBSD, step size of 70 nm). The EBSD results were post analyzed by MTEX reconstruction to determine the PAGBs [34]. Data points with low CI values ($>$0.05) were considered as noise points due to the high dislocation density and therefore corrected. Uniaxial tensile tests were performed at a constant crosshead speed of 0.2 mm/min. Tensile strains were measured using a strain gauge extensometer (Shimadzu SG10-100). Two types of tensile specimens, as depicted in Fig. 1 (b), were fabricated to determine the tensile properties (b1) and to perform in situ observations for deformation (b2).

The bainite and as-quenched martensite microstructure were distinguished by their different resistance to chemical etching. Specifically, a 1-s etching by a 2% Nital etchant was performed on as-quenched specimens, followed by optical microscope (OM) and SEM observations. Nital etches the bainitic regions within a short time, whereas as-quenched martensite and RA remain less etched [35]. A detailed description is provided in the supplementary material.

Table 1
Chemical composition of the high-carbon steel used in this study (wt.%). Elements less than 0.02 wt% are not listed.

C	Si	Mn	Cr	Mo	V	Al	Fe
0.834	1.78	1.79	1.18	0.32	0.09	0.056	Bal.

3. Results and discussions

Fig. 2 depicts the microstructure of the B/M specimens after a 10-min isothermal holding at 300 ° C. In Fig. 2 (a), the etched dark regions correspond to the bainite sheaves, while the bright areas represent less-etched martensite and RA. Overall, a low fraction of lower bainite was observed after 10 min of isothermal holding, where most bainite sheaves nucleated along PAGBs, as shown in Fig. 2(b4) and 2(c4). This is because the PAGBs provide high-energy sites for potential bainite nucleation, while the bainite sheaves subsequently grow and thicken along these PAGBs.

Fig. 2(b) and (c) exhibit the morphology of lower bainite sheaves along a curved PAGB and a linear PAGB. In Fig. 2(b1), the bainite sheaf consists of thin parallel subunits, separated by film austenite. This forms a curved bainite sheaf with a uniform thickness less than 1 μm along the curved PAGB. Notably, the lower bainite did not fully cover all PAGBs in the present B/M specimens, due to the low bainitic transformation time. Instead, bainite preferentially nucleated along high-energy PAGBs which provide potential premature crack initiation sites [10,36]. Compared with the lower bainite sheaves grown within PAGs, the present bainite along PAGBs exhibited thinner substructure and morphology dependent on local boundary [37]. It is inferred that such bainitic transformation leads to an effective enhancing effect on high-energy PAGBs.

Fig. 2(b3) and 2(c3) show that blocky RA grains are distributed around the bainite sheaves. Due to the suppression of carbide precipitation by Si, carbon diffusion from bainite to surrounding austenite is enhanced. During oil quenching, martensitic transformation preferentially occurs in low-carbon austenite regions, whereas the transformation in carbon enrichment regions require higher degree of undercooling. Furthermore, carbon diffusion from bainite to RA, particularly during the tempering process, stabilizes local blocky RA grains.

Fig. 3 depicts the tensile properties of the full M and B/M specimens. In Fig. 3(a), most full M specimens showed brittle fractures within the elastic regime. Poor ductility was observed regardless of the post tempering conditions. Conversely, the B/M specimens exhibit notable plastic deformation, as shown in Fig. 3(b). With a 10-min holding at 280 ° C (red curve), the ductility was significantly improved due to strain hardening deformation. A prolonged bainitic transformation (blue curve) leads to a slight decrease of the ultimate strength and improved ductility. Additionally, the 300° C specimen (green curve) exhibited much decreased yield strength while higher work hardening rate. Fig. 3 (c) shows the effect of bainitic transformation time at 280 ° C on the fracture strain and strength, revealing a brittle-to-ductile transition at the early stage of bainitic transformation.

Fig. 3(d) compares the tensile properties of the present B/M specimens with those of recently developed ultra-high strength steels [1,4,6, 15,17,23,38–57]. The results show that the present B/M specimens occupy a distinct area in the strength-ductility domain. Compared to other bulk B/M steels [17,53–55], the high-carbon B/M specimens achieve an approximate 500 MPa increase in ultimate tensile strength while maintaining equivalent elongations. Notably, compared to some ultrahigh-strength steels utilizing severe deformation for nano-grained microstructure [38,44,58], the present superior mechanical properties were achieved by only heat treatment and low content of costly alloying elements.

To elucidate the deformation mechanism of the B/M microstructure, in situ EBSD analysis was performed during the uniaxial tensile deformation. Fig. 4 illustrates the deformation mechanisms of the B/M specimens (300°C, 10 min) in various stages of the tensile response. Throughout the tensile process, the overall PAGs exhibited slight distortion, whereas the intragranular substructure underwent significant deformation.

In the initial microstructure, blocky RA grains distributed between the bainite and martensite blocks (after the tempering process, it is

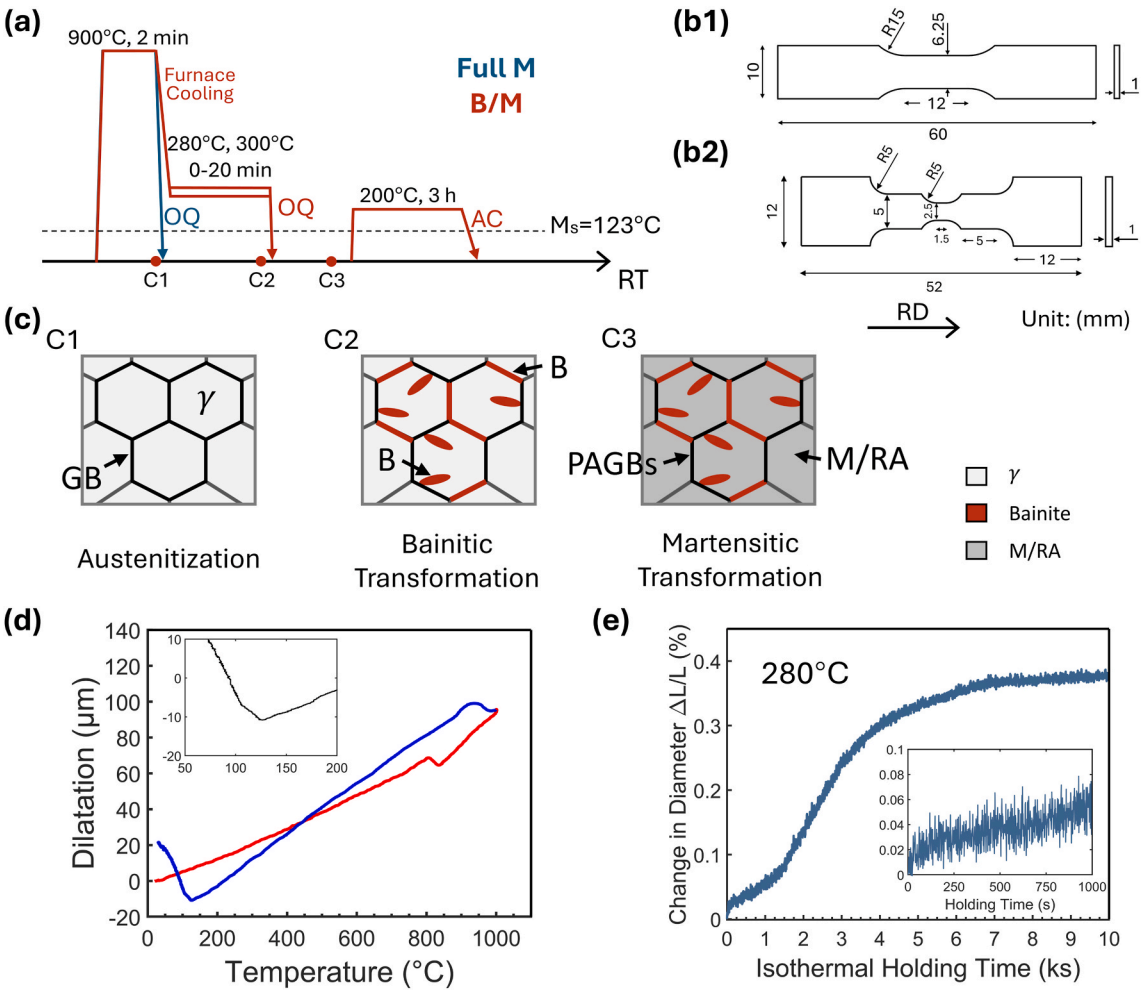

Fig. 1. (a) Heat treatment processes of the B/M group (red) and full M group (blue) specimens. OQ and AC represent oil quenching and air cooling. Two types of tensile specimens were fabricated for (b1) tensile properties and (b2) in situ observation purposes. (c) Schematics of the microstructure evolution of the B/M specimens at different heat treatment stages as shown in (a). (d) The dilatation curve of an 8 mm-diameter specimen with heating rate of 30 ° C/s to 1000° C and a cooling rate of at 20° C/s by nitrogen gas quenching. (e) The dilatation curve under isothermal holding at 280° C after heating up to 900° C for 2 min. (For interpretation of the references to colour in this figure legend, the reader is referred to the Web version of this article.)

difficult to distinguish between bainite and martensite). In the early deforming stage at 2.3% strain, the overall microstructure did not exhibit obvious deformation. Notably, the slight distortion of the blocky RA was observed between 0% and 2.3% which is mainly attributed to the noise correction. As the tensile strain further increased to 5.4%, The volume fraction of RA rapidly dropped from 12.9% to 5.6%, attributed to deformation induced martensitic transformation (DIMT). At tensile strain of 7.8%, the RA fraction further decreased to 3.4% under an ultrahigh stress of 2.6 GPa. It is inferred that the excellent RA stability under ultrahigh strength is associated with the carbon diffusion during the tempering processes [59]. Overall, the martensitic block size seems to slightly grow accompanying with the tensile deformation. The TRIP effect corresponds to the strain-hardening stage of the present B/M microstructure.

The misorientation profiles from point P1 to P2 demonstrate DIMT behaviour: the blocky RA grain γ continuously shrinks, accompanied by the evolution of the martensite grain M-2. This indicates that the martensitic transformation always occurs at RA/M interfaces and exhibits the same orientation to the adjacent martensite grain [60,61]. This observation aligns with the deformation-induced grain rotation behaviour of blocky RA grains [62]. Notably, minor grain rotations were also observed in some martensite blocks, which tended to mitigate the misorientation with adjacent blocks [63]. Moreover, such fcc-to-bcc transformation-induced-plasticity (TRIP) effect significantly contributes to the work-hardening response as observed in Fig. 3(b) [64]. The deformation of blocky RA and martensite blocks provides plasticity, while the BFs enhance the PAGBs from premature fracture. Consequently, both the TRIP effect and PAGB enhancement by bainite formation are responsible for the improved ductility and ultrahigh strength in the B/M specimens.

Fig. 5 illustrates the plastic deformation and fracture mechanisms of the full M and B/M specimens. In the full M group, tempered martensite and RA grains dominate the substructure, while the atomic mobility at PAGBs is hindered. Under high tensile stress, the boundaries tend to separate without adequate plastic deformation, resulting in early crack initiation at PAGBs [65]. In Fig. 5, the fracture surface of the full M specimen is characterized by intergranular brittle fracture patterns with a small portion of localized dimples. This indicates that PAGBs behave as the premature brittle sites in the low-temperature-tempered (LTT) high-carbon martensite [6,66].

In contrast, the B/M specimens exhibit a well-deformed fracture surface with a relatively homogeneous morphology. The sub-μm patterns of concave lumps, neither dimple nor cleavage, correspond to localized rupture fractures after sufficient ductile deformation. Although the fracture patterns also exhibit some river-like fluctuations, no flat PAGB pattern was observed along the boundaries, indicating an effective PAGB enhancement effect in the B/M specimens.

The PAGB enhancement mechanism facilitated by bainite

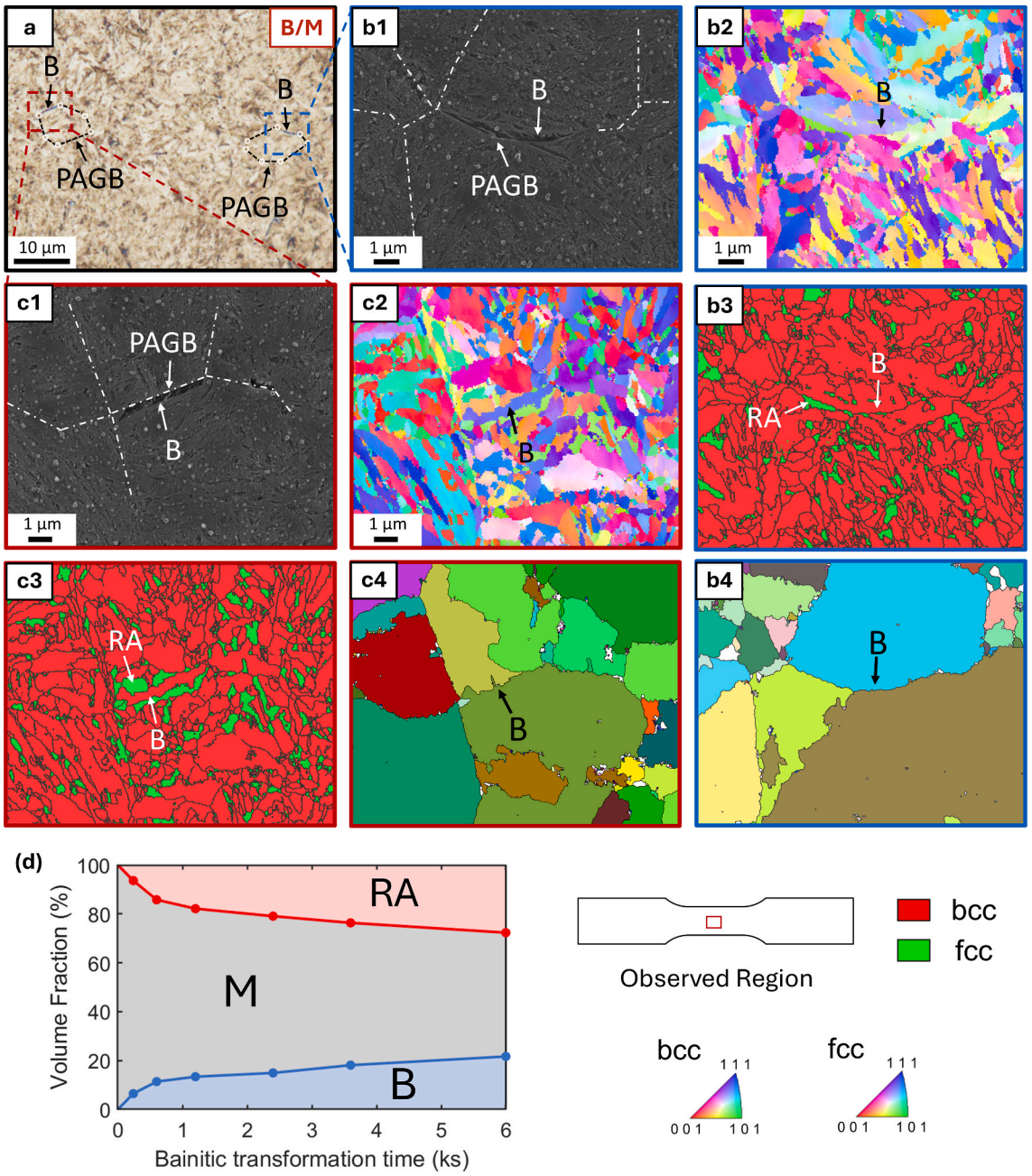

Fig. 2. (a) Optical microscope (OM) observation on the as-quenched B/M specimen. (b1-b3) The SEM observation, IPF map and phase map of a bainite sheaf along a curved PAGB as shown in the blue region in Fig. 2(a). (c1-c3) The SEM observation, IPF map and phase map of a bainite sheaf along a straight PAGB as shown in the red region in Fig. 2(a). (b4) and (c4) show the prior austenite reconstruction maps for the two selected regions. (d) The volume fraction evolution of bainite, martensite and retained austenite (RA) with bainitic transformation times at 280 ° C. (For interpretation of the references to colour in this figure legend, the reader is referred to the Web version of this article.)

transformation is demonstrated in Fig. 5. Lower bainite nucleates along one side of PAGBs, while blocky RA grains are widely observed adjacent to the PAGBs and bainite sheaves [67]. The bainite and RA grains with higher plastic deformability occupy the PAGBs with higher GB energies, suppressing local premature crack initiation [11,68]. Additionally, the blocky RA grains can also transform into bcc martensite under the TRIP effect, dissipating local residual stress and further enhancing PAGBs. The difference in fracture mechanisms between full M and B/M specimens is attributed to the deformability difference of martensite and bainite/RA grains at PAGBs.

4. Conclusions

In conclusion, the present study proposes a novel fabrication route for lean, ultrastrong yet ductile bainite/martensite microstructure, achieving a superior combination of an ultimate tensile strength of 2.64 GPa and an elongation of over 10%. A low portion of prior lower bainite was obtained within short transformation times by slow furnace cooling. Compared to the full M specimens which exhibited early brittle fracture, the lower bainite sheaves and RA grains along PAGBs in the B/M specimens improved local deformability and prevented early crack initiation. The strain hardening behaviour is associated with the TRIP effect of RA grains, and slight grain rotation was also observed under high stress.

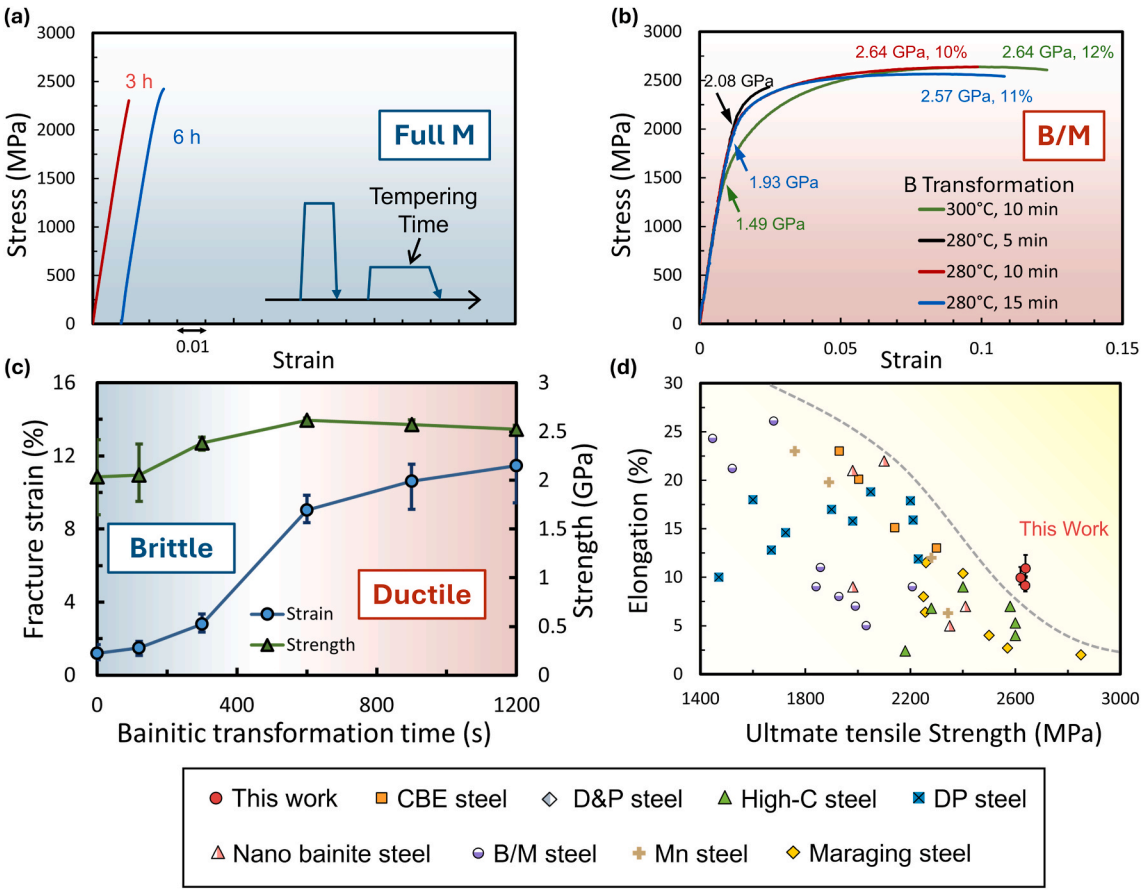

Fig. 3. Stress strain curves of the (a) full M specimens with various tempering times and (b) B/M specimens with various bainitic transformation temperatures and times. (c)The effect of bainitic transformation time at 280 ° C on the evolution fracture strains. (d) A comparison of the strength-ductility combinations between this work and other ultrahigh-strength steels, including chemical boundary engineering (CBE) steels [38], maraging steels [4,39–43], high-carbon steels [6,44,45], M/ γ dual phase (DP) steels [1,46–49], nano bainite steels [15,50–52], B/M steels [17,23,53–55], medium-Mn steels [56] and deformed and partitioned (D&P) steels [57].

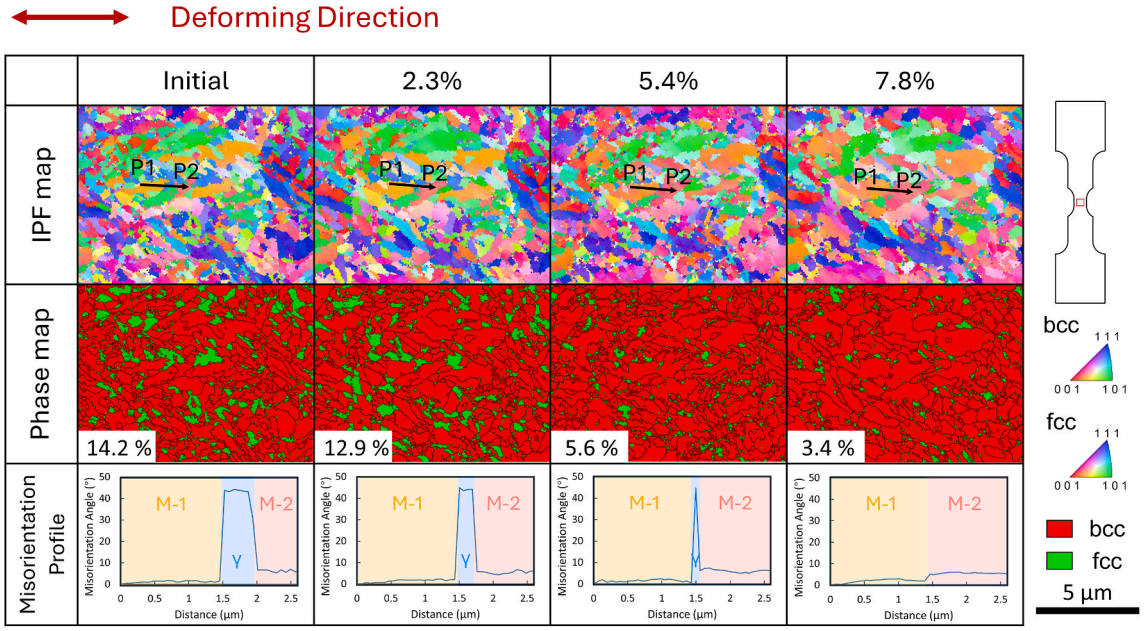

Fig. 4. EBSD analyses (IPF maps and phase maps) of the B/M microstructure in the in-situ tensile specimen at different strains of 0%, 2.3%, 5.4%, and 7.8%. The heat treatment process is 900 ° C, 2 min - 300° C, 10 min - OQ - 200° C, 3 h. The volume fraction of RA was labeled at the bottom-left corner of each phase map, and the point-to-origin misorientation angle profiles of P1 to P2 are shown in each chart. Slight distortions of the grains attribute to the noise correction.

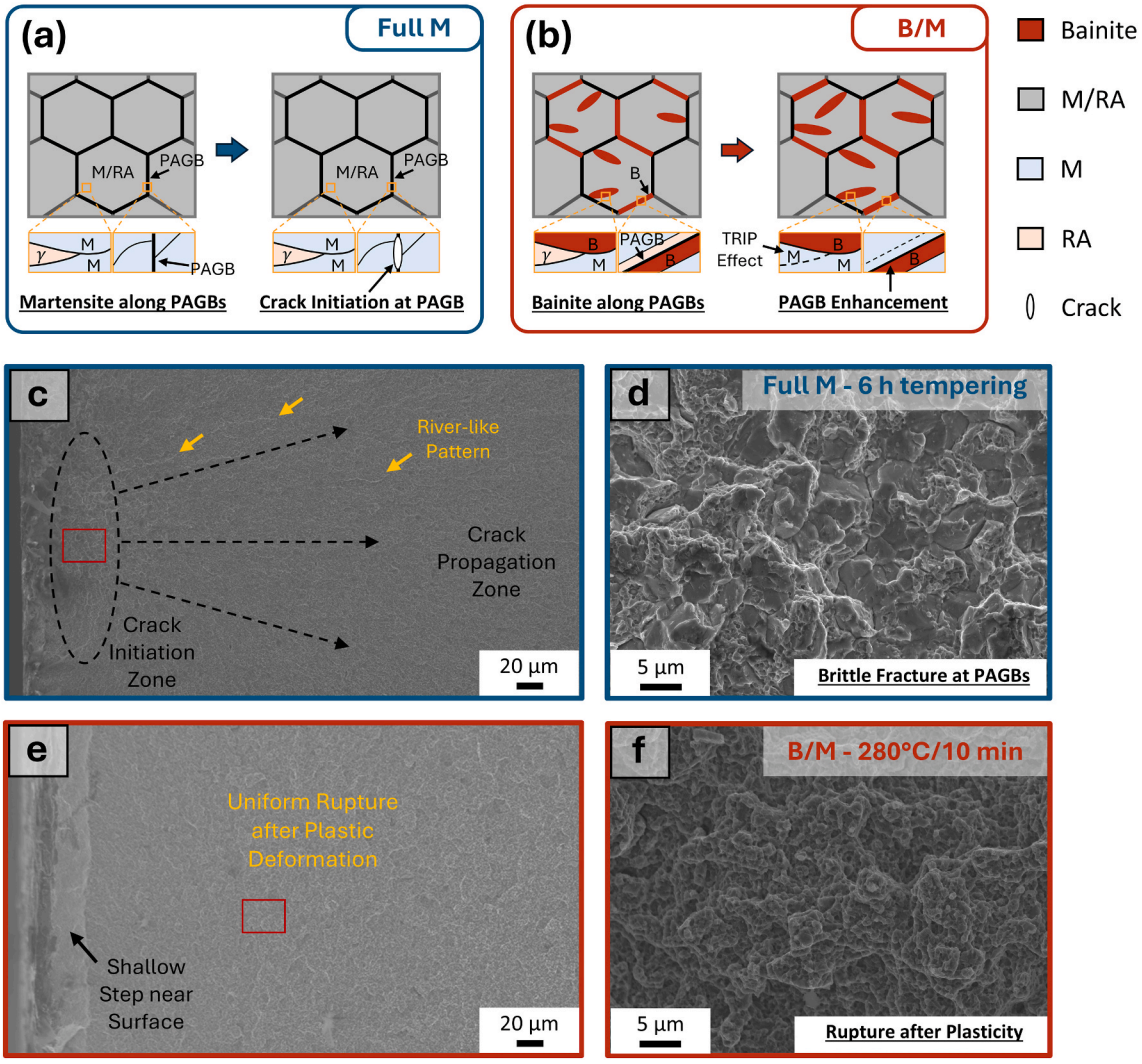

Fig. 5. Schematics and the deformation and fracture mechanisms of (a) the full M and (b) the B/M specimens. The full M specimens exhibit early brittle crack initiation at PAGBs, and the B/M specimens show deformation of bainite sheaves. (c) SEM observation on the fracture surface of the full M – 6 h specimen. (d) Zoomed in observation on the crack initiation spot as labeled in (c). (e) SEM observation on the fracture surface of the B/M – 280 ° C/10 min specimen. (f) Zoomed in observation on the uniform rupture region.

Moreover, a low fraction of lower bainite can effectively enhance the PAGBs of martensite without sacrificing its ultrahigh strength, offering a strategy for achieving superior strength-ductility combination.

CRediT authorship contribution statement

Sien Liu: Writing – original draft, Software, Methodology, Investigation, Formal analysis, Data curation, Conceptualization. **Koyo Shimizu:** Software, Investigation, Data curation. **Jiaqiang Dang:** Methodology, Investigation. **Karel Blanken:** Software, Data curation. **Fabien Briffod:** Software, Methodology, Data curation. **Shoichi Nambu:** Writing – review & editing, Supervision, Resources, Project administration, Funding acquisition, Conceptualization.

Originality statement

I write on behalf of myself and all co-authors to confirm that the results reported in the manuscript are original and neither the entire work, nor any of its parts have been previously published. The authors confirm that the article has not been submitted to peer review, nor has been accepted for publishing in another journal. The author(s) confirms that the research in their work is original, and that all the data given in the article are real and authentic. If necessary, the article can be recalled, and errors corrected.

Declaration of competing interest

The authors declare that they have no known competing financial interests or personal relationships that could have appeared to influence the work reported in this paper.

Appendix A. Supplementary data

Supplementary data to this article can be found online at https://doi.org/10.1016/j.msea.2026.149955.

Data availability

Data will be made available on request.

References

[1] Y. Li, G. Yuan, L. Li, J. Kang, F. Yan, P. Du, D. Raabe, G. Wang, Ductile 2-GPa steels with hierarchical substructure, Science 379 (2023) 168–173.

[2] Z. Shang, T. Sun, J. Ding, N.A. Richter, N.M. Heckman, B.C. White, B.L. Boyce, K. Hattar, H. Wang, X. Zhang, Gradient nanostructured steel with superior tensile plasticity, Sci. Adv. 9 (2023) eadd9780.
[3] Y.-Q. Yan, W.-H. Cha, S. Liu, Y. Ma, J.-H. Luan, Z. Rao, C. Liu, Z.-W. Shan, J. Lu, G. Wu, Ductilization of 2.6-GPa alloys via short-range ordered interfaces and supranano precipitates, Science 387 (2025) 401–406.
[4] T. Liu, Z. Cao, H. Wang, G. Wu, J. Jin, W. Cao, A new 2.4 GPa extra-high strength steel with good ductility and high toughness designed by synergistic strengthening of nano-particles and high-density dislocations, Scr. Mater. 178 (2020) 285–289.
[5] J.-j. Sun, Y.-n. Liu, Y.-t. Zhu, F.-l. Lian, H.-j. Liu, T. Jiang, S.-w. Guo, W.-q. Liu, X.-b. Ren, Super-strong dislocation-structured high-carbon martensite steel, Sci. Rep. 7 (2017) 6596.
[6] Y. Wang, J. Sun, T. Jiang, Y. Sun, S. Guo, Y. Liu, A low-alloy high-carbon martensite steel with 2.6 GPa tensile strength and good ductility, Acta Mater. 158 (2018) 247–256.
[7] L. Junkui, Y. Zhinan, M. Hua, C. Chen, Z. Fucheng, A medium-C martensite steel with 2.6 GPa tensile strength and large ductility, Scr. Mater. 228 (2023) 115327.
[8] T. Sakamaki, M. Tanaka, T. Morikawa, H. Nako, S. Nanba, Brittle-to-ductile transition in martensite – bainite steel, ISIJ Int. 61 (2021) 2167–2175.
[9] K. Chen, H. Li, Z. Jiang, F. Liu, C. Kang, X. Ma, B. Zhao, Multiphase microstructure formation and its effect on fracture behavior of medium carbon high silicon high strength steel, J. Mater. Sci. Technol. 72 (2021) 81–92.
[10] J.H. Kim, G. Miyamoto, A. Shibata, T. Hojo, M. Koyama, Y. Zhang, T. Furuhara, Influence of austenite grain boundary misorientation on hydrogen-induced intergranular crack propagation in a medium carbon martensitic steel, Acta Mater. 274 (2024) 120036.
[11] S. Jimbo, S. Nambu, Crystallographic analysis on the lower bainite formation at the austenite grain boundary in Fe-0.6C-0.8Mn-1.8Si steel in the initial stage of transformation, ISIJ Int. 64 (2024) 338–344.
[12] K. Abbaszadeh, H. Saghafian, S. Kheirandish, Effect of bainite morphology on mechanical properties of the mixed bainite-martensite microstructure in D6AC steel, J. Mater. Sci. Technol. 28 (2012) 336–342.
[13] H.-B. Lee, H.H. Lee, Y.-B. Song, J. Ham, Y.J. Kim, H.-K. Kim, D.-W. Suh, Influence of chronological control of transformation on the microstructure and mechanical properties of complex phase steels, Scr. Mater. 200 (2021) 113892.
[14] J. Tian, G. Xu, Z. Jiang, Q. Yuan, G. Chen, H. Hu, Effect of austenisation temperature on bainite transformation below martensite starting temperature, Mater. Sci. Technol. 35 (2019) 1539–1550.
[15] F.G. Caballero, H.K.D.H. Bhadeshia, Very strong bainite, Curr. Opin. Solid State Mater. Sci. 8 (2004) 251–257.
[16] T. Sourmail, V. Smanio, Low temperature kinetics of bainite formation in high carbon steels, Acta Mater. 61 (2013) 2639–2648.
[17] X.-p. Yu, H.-b. Wu, Y. Gu, R. Yuan, Y.-y. Zhang, Y.-h. Feng, Effect of prior martensite on bainite transformation and microstructure of high-carbon nano-bainitic steel, J. Iron Steel Res. Int. 29 (2022) 647–654.
[18] W. Gong, Y. Tomota, S. Harjo, Y.H. Su, K. Aizawa, Effect of prior martensite on bainite transformation in nanobainite steel, Acta Mater. 85 (2015) 243–249.
[19] S. Das, A. Haldar, Continuously cooled ultrafine bainitic steel with excellent strength–elongation combination, Metall. Mater. Trans. A 45 (2014) 1844–1854.
[20] T. Kaneshita, G. Miyamoto, T. Furuhara, Variant selection in grain boundary nucleation of bainite in Fe-2Mn-C alloys, Acta Mater. 127 (2017) 368–378.
[21] X. Lu, Z. Yang, D. Qian, J. Lan, L. Hua, Effect of martensite pre-quenching on bainite transformation kinetics, martensite/bainite duplex microstructures, mechanical properties and retained austenite stability of GCr15 bearing steel, J. Mater. Res. Technol. 15 (2021) 2429–2438.
[22] S. Samanta, P. Biswas, S. Giri, S.B. Singh, S. Kundu, Formation of bainite below the MS temperature: kinetics and crystallography, Acta Mater. 105 (2016) 390–403.
[23] F.G. Caballero, J. Chao, J. Cornide, C. García-Mateo, M.J. Santofimia, C. Capdevila, Toughness deterioration in advanced high strength bainitic steels, Mater. Sci. Eng., A 525 (2009) 87–95.
[24] F. Zhao, L. Morales-Rivas, Q. Yu, G. Wang, F.G. Caballero, D. San-Martin, Unforeseen influence of the prior austenite grain size on the mechanical properties of a carbide-free bainitic steel, Mater. Sci. Eng., A 881 (2023) 145388.
[25] J. Bai, S. Jin, C. Liang, X. Li, Z. You, Y. Zhao, L. Liu, G. Sha, Microstructural origins for quench cracking of a boron steel: boron distribution, Mater. Char. 190 (2022) 112022.
[26] Z. Jiang, Y. Li, Z. Yang, P. Wang, D. Li, Y. Li, The tempering behavior of martensite/austenite islands on the mechanical properties of a low alloy Mn-Ni-Mo steel with granular bainite, Mater. Today Commun. 26 (2021) 102166.
[27] A.M. Ravi, J. Sietsma, M.J. Santofimia, The role of grain-boundary cementite in bainite formation in high-carbon steels, Scr. Mater. 185 (2020) 7–11.
[28] L. Liu, L. Li, J. He, Z. Liang, Z. Peng, J. Gao, Z. Luo, M. Huang, The unexpected low fracture toughness of dual-phase steels caused by ferrite/martensite interface decohesion, Scr. Mater. 244 (2024) 116030.
[29] L. Liu, L. Li, Z. Liang, M. Huang, Z. Peng, J. Gao, Z. Luo, Towards ultra-high strength dual-phase steel with excellent damage tolerance: the effect of martensite volume fraction, Int. J. Plast. 170 (2023) 103778.
[30] A. Shibata, T. Katsuno, M. Tsuboi, N. Tsuji, Effect of bain unit size on low-temperature fracture toughness in medium-carbon martensitic and bainitic steels, ISIJ Int. 64 (2024) 381–388.
[31] C. Garcia-Mateo, H.K.D.H. Bhadeshia, Nucleation theory for high-carbon bainite, Mater. Sci. Eng., A 378 (2004) 289–292.
[32] S. Lin, A. Borgenstam, A. Stark, P. Hedström, Effect of Si on bainitic transformation kinetics in steels explained by carbon partitioning, carbide formation, dislocation densities, and thermodynamic conditions, Mater. Char. 185 (2022) 111774.
[33] M. Morawiec, J. Opara, C. Garcia-Mateo, J.A. Jimenez, A. Grajcar, Effect of Mn on the chemical driving force and bainite transformation kinetics in medium-manganese alloys, J. Therm. Anal. Calorim. 148 (2023) 1567–1576.
[34] F. Niessen, T. Nyyssonen, A.A. Gazder, R. Hielscher, Parent grain reconstruction from partially or fully transformed microstructures in MTEX, J. Appl. Crystallogr. 55 (2022) 180–194.
[35] A.M. Ravi, A. Navarro-López, J. Sietsma, M.J. Santofimia, Influence of martensite/austenite interfaces on bainite formation in low-alloy steels below Ms, Acta Mater. 188 (2020) 394–405.
[36] L. Lan, Z. Chang, P. Fan, Exploring the difference in bainite transformation with varying the prior austenite grain size in low carbon steel, Metals 8 (2018) 988.
[37] A.M. Ravi, J. Sietsma, M.J. Santofimia, Exploring bainite formation kinetics distinguishing grain-boundary and autocatalytic nucleation in high and low-Si steels, Acta Mater. 105 (2016) 155–164.
[38] R. Ding, Y. Yao, B. Sun, G. Liu, J. He, T. Li, X. Wan, Z. Dai, D. Ponge, D. Raabe, C. Zhang, A. Godfrey, G. Miyamoto, T. Furuhara, Z. Yang, S. van der Zwaag, H. Chen, Chemical boundary engineering: a new route toward lean, ultrastrong yet ductile steels, Sci. Adv. 6 (2020) eaay1430.
[39] M. Niu, G. Zhou, W. Wang, M.B. Shahzad, Y. Shan, K. Yang, Precipitate evolution and strengthening behavior during aging process in a 2.5 GPa grade maraging steel, Acta Mater. 179 (2019) 296–307.
[40] F. Guo, M. Wang, P. Ye, Y. Zhai, C. Zhang, Q. Cheng, W. Su, Q. Wang, J. Liang, W. Cao, C. Huang, Achieving good ductility in 2.1 GPa grade maraging steel, Mater. Sci. Eng., A 890 (2024) 145886.
[41] S. Jiang, H. Wang, Y. Wu, X. Liu, H. Chen, M. Yao, B. Gault, D. Ponge, D. Raabe, A. Hirata, M. Chen, Y. Wang, Z. Lu, Ultrastrong steel via minimal lattice misfit and high-density nanoprecipitation, Nature 544 (2017) 460–464.
[42] J. Wan, H. Ruan, Z. Ding, L.B. Kong, A novel maraging stainless steel ultra-high-strengthened by multi-nanoprecipitations, Scr. Mater. 226 (2023) 115224.
[43] Z. Liu, Z. Yang, X. Wang, J. Liang, Z. Yang, H. Wu, G. Sha, Enhanced strength-ductility synergy in a new 2.2 GPa grade ultra-high strength stainless steel with balanced fracture toughness: elucidating the role of duplex aging treatment, J. Alloys Compd. 928 (2022) 167135.
[44] J. Wang, Q. Tao, J. Fan, L. Fu, A. Shan, Enhanced mechanical properties of a high-carbon martensite steel processed by heavy warm rolling and tempering, Mater. Sci. Eng., A 872 (2023) 144958.
[45] J. Sun, T. Jiang, Y. Wang, S. Guo, Y. Liu, Effect of grain refinement on high-carbon martensite transformation and its mechanical properties, Mater. Sci. Eng., A 726 (2018) 342–349.
[46] J. Wang, S. Wang, W. Li, Y. Yao, X. Wang, Z. Yang, H. Chen, Ultrastrong and ductile additively-manufactured medium-carbon steel via modulating austenite stability, Scr. Mater. 239 (2024) 115780.
[47] R. Ueji, K. Nagata, H. Somekawa, M. Demura, Application of a sparse mixed regression method to design the optimal composition and heat treatment conditions for transformation-induced plasticity steel with high strength and large elongation, Scr. Mater. 222 (2023) 115028.
[48] G. Niu, D. Jin, Y. Wang, H. Chen, N. Gong, H. Wu, Achieving 2.2 GPa ultra-high strength in low-alloy steel using a direct quenching and partitioning process, Materials 16 (2023) 7533.
[49] C.P. Scott, B. Shalchi Amirkhiz, I. Pushkareva, F. Fazeli, S.Y.P. Allain, H. Azizi, New insights into martensite strength and the damage behaviour of dual phase steels, Acta Mater. 159 (2018) 112–122.
[50] J. Tian, G. Xu, Z. Jiang, H. Hu, M. Zhou, Effect of Ni addition on bainite transformation and properties in a 2000 MPa grade ultrahigh strength bainitic steel, Met. Mater. Int. 24 (2018) 1202–1212.
[51] H.K.D.H. Bhadeshia, Nanostructured bainite, Proc. R. Soc. A 466 (2010) 3–18.
[52] J. Behzadifar, S. Mohammad-Ali Boutorabi, H. Saghafian Larijani, Effects of austempering on the microstructure and mechanical properties of high-strength nanostructured bainitic steel containing 3.5 wt% aluminum, J. Mater. Res. Technol. 29 (2024) 344–352.
[53] G. Mandal, C. Roy, S.K. Ghosh, S. Chatterjee, Structure-property relationship in a 2 GPa grade micro-alloyed ultrahigh strength steel, J. Alloys Compd. 705 (2017) 817–827.
[54] X. Zhou, T. Zeng, X. Shi, M. Zhao, W. Wang, Y. Li, W. Yan, An ultra-high strength bainitic aging steel, Scr. Mater. 245 (2024) 116061.
[55] T. Zhang, Y. Wang, C. Wang, B. Mi, X. You, L. Wang, H. Chen, Z. Yang, W. Xu, C. Zhang, A heterostructured bainitic steel produced by two-step austempering and low-temperature ausforming, Scr. Mater. 242 (2024) 115943.
[56] Y. Li, L. Li, J. Kang, N. Niu, H. Xi, Y. Liu, G. Yuan, G. Wang, Achieving unprecedented yield strength of 2.2 GPa with high ductility in formed parts using strain-aging, Scr. Mater. 233 (2023) 115521.
[57] B.B. He, B. Hu, H.W. Yen, G.J. Cheng, Z.K. Wang, H.W. Luo, M.X. Huang, High dislocation density–induced large ductility in deformed and partitioned steels, Science 357 (2017) 1029–1032.
[58] F. Guo, C. Zhang, Y. Zhai, Q. Cheng, M. Wang, Q. Wang, J. Liang, W. Cao, C. Huang, Nanosized austenite and coherent nanoprecipitates making maraging steel strong and ductile, Mater. Sci. Eng., A 902 (2024) 146605.
[59] X.Y. Long, D.Y. Sun, K. Wang, F.C. Zhang, Z.N. Yang, Y.G. Li, C.L. Zheng, Effect of carbon distribution range in mixed bainite/martensite/retained austenite microstructure on mechanical properties, J. Mater. Res. Technol. 17 (2022) 898–912.
[60] K. Kanetani, T. Moronaga, T. Hara, K. Ushioda, Deformation-induced martensitic transformation behavior of retained austenite during rolling contact in carburized SAE4320 steel, ISIJ Int. 61 (2021) 2629–2635.

[61] H. Na, S. Nambu, M. Ojima, J. Inoue, T. Koseki, Crystallographic and microstructural studies of lath martensitic steel during tensile deformation, Metall. Mater. Trans. A 45 (2014) 5029–5043.
[62] C. Du, Y. Gao, M. Zha, C. Wang, H. Jia, H.-Y. Wang, Deformation-induced grain rotation and grain boundary formation achieved through dislocation-disclination reactions in polycrystalline hexagonal close-packed metals, Acta Mater. 250 (2023) 118855.
[63] H. Na, S. Nambu, M. Ojima, J. Inoue, T. Koseki, Strain localization behavior in low-carbon martensitic steel during tensile deformation, Scr. Mater. 69 (2013) 793–796.
[64] E.I. Galindo-Nava, P.E.J. Rivera-Díaz-del-Castillo, Understanding martensite and twin formation in austenitic steels: a model describing TRIP and TWIP effects, Acta Mater. 128 (2017) 120–134.
[65] F. Archie, S. Zaefferer, On variant selection at the prior austenite grain boundaries in lath martensite and relevant micro-mechanical implications, Mater. Sci. Eng., A 731 (2018) 539–550.
[66] D.B.V.d. Castro, J.M. Ventura, C.O.F.T. Ruckert, D. Spinelli, W.W. Bose Filho, Influence of phosphorus content and quenching/tempering temperatures on fracture toughness and fatigue life of SAE 5160 steel, Mater. Res. 13 (2010).
[67] R. Ranjan, S.B. Singh, Isothermal bainite transformation in low-alloy steels: mechanism of transformation, Acta Mater. 202 (2021) 302–316.
[68] A.K. Chandan, G.K. Bansal, J. Kundu, J. Chakraborty, S.G. Chowdhury, Effect of prior austenite grain size on the evolution of microstructure and mechanical properties of an intercritically annealed medium manganese steel, Mater. Sci. Eng., A 768 (2019) 138458.